Guillaume, B., Pochat, S., Monteux, J., Husson, L., and Choblet, G., 2016, Can eustatic charts go beyond first order? Insights from the Permian–Triassic: Lithosphere, doi:10.1130/L523.1.

Numerical model set-up

We assume that the mantle deforms in a diffusion creep limit. We assume an incompressible medium with an infinite Prandtl number. The dynamic equations are solved in an axi-symmetric spherical geometry using 100×200 grid points in the r and θ directions. An implicit inversion method [Schubert et al., 2001] is adopted for the momentum equation, and an Alternating Direction Implicit scheme [Peaceman and Rachford, 1955; Douglas, 1955] for the energy and mass conservation. Free-slip velocity is imposed at the surface and along the axis of symmetry.

Since the geometry of the the problem is axi-symmetric (mantle plume flowing below a super-continent), both 3D and 2D axi-symmetric models are appropriate. Differences may eventually arise in 2 cases: (1) in 2D-axi-symmetric models when the subduction starts at the super-continent margins since a single planetary scale axi-symmetric slab is unlikely and (2) in 3D cartesian models when the effect of curvature is not accounted [see e.g., Jarvis et al., 1995; O'Farrell et al., 2013]. In our study, the point (2) is correctly characterized in our spherical geometry models. Concerning point (1), since we focus here on the dynamic topography effect of a large mantle plume below a super-continent, the validity of our models is correct during the first 50 Myr.

To illustrate the influence of a rising mantle plume on the dynamic topography of an aggregated supercontinent and its interactions with large scale sinking slabs, we consider the following initial set-ups: (1) initially neither hot mantle plume nor dense oceanic lithosphere are considered (2) a dense oceanic lithosphere is included in the model without a large mantle plume (3) a dense oceanic lithosphere and a mantle plume at the core-mantle boundary (CMB) are included in the model. In our numerical models, the temperature is set to 273K above the oceanic lithosphere while the supercontinent is simply considered as a cap with an extension of 60° of latitude and zero heat flux. The mantle plume is initiated by imposing a cap-shape thermal anomaly at the CMB along the symmetry axis. We consider an initial cap-shape thermal anomaly with lateral extensions of 40° above the CMB (Fig. 1). This initially large thermal anomaly rapidly gathers along the symmetry axis within a plume with a head lateral extension of 10-15°.

From our numerical models we can monitor the flow dynamics within the mantle and, hence, the corresponding dynamic topography h that is:

$$h = \frac{2\eta}{\Delta\rho g}\frac{dv}{dr} \tag{1}$$

where η is the mantle viscosity, g is the gravitational acceleration and dv/dr is the surface radial velocity gradient. Negative dynamic topography is generally restricted to the oceanic part of the model and we consider that the mantle material is compensated with water and $\Delta\rho = 2500$ kg.m^{-3}. Positive dynamic topography is generally restricted to the continental part of the model and we consider that the mantle material is compensated with air and $\Delta\rho = 3500$ kg.m^{-3}. Note that in the case where negative topography could be adjacent to air in some regions and positive topography could be adjacent to water in other regions, the values reported in Fig. 7 would be overestimated/underestimated by 40%.

We characterize the thermo-chemical readjustment that occurs during the plume ascension induced by the cap-shape thermal anomaly at the CMB (Fig. 1). The ascension of the thermal plume is followed by its spreading below the insulating continent (Fig. 1, middle). During this spreading, the thermal plume flattens until its thickness reaches a value for which motionless thermal diffusion becomes more effective than advection. Then, the thermal anomaly cools by conduction and heat is diffused in all direction within the surrounding mantle. In the meantime, the colder (and denser) oceanic lithosphere forms a viscous slab that sinks toward the core-mantle boundary within a slightly longer timescale. Later, another cold slab is initiated at the cooling surface (Fig. 1, right).

Figure 1: Thermal readjustment as a function of time (from left to right) during the ascension of a thermal plume initiated by a 40° thermal anomaly at the core-mantle boundary.

References

Douglas, J., 1955. On the numerical integration of $\frac{\partial^2 u}{\partial x^2} + \frac{\partial^2 u}{\partial y^2} = \frac{\partial u}{\partial t}$ by implicit methods. J. Soc. Ind. Appl. Math. 3, 42–65.

Jarvis, G. T., Glatzmaier, G. A., Vangelov, V. I., 1995. Effects of curvature, aspect ratio and plan form in two- and three-dimensional spherical models of thermal convection. Geophysical and Astrophysical Fluid Dynamics 79, 147–171.

O'Farrell, K. A., Lowman, J. P., Bunge, H.-P., Feb. 2013. Comparison of spherical-shell and plane-layer mantle convection thermal structure in viscously stratified models with mixed-mode heating: implications for the incorporation of temperature-dependent parameters. Geophysical Journal International 192, 456–472.

Peaceman, D. W., Rachford, H. H., 1955. The numerical solution of parabolic and elliptic differential equations. J. Soc. Ind. Appl. Math. 3, 28–41.

Schubert, G., Turcotte, D. L., Olson, P., Sep. 2001. Mantle convection in the Earth and planets. Cambridge University Press.

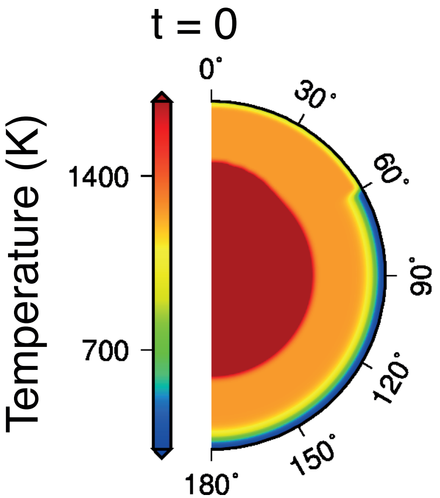

t = 0
t = 20 m.y.
t = 50 m.y.
Temperature (K)
1400
700
0°
30°
60°
90°
120°
150°
180°